Sharif University of Technology

Scientia Iranica

Transactions on Computer Science & Engineering and Electrical Engineering

https://scientiairanica.sharif.edu

Design and implementation of class-E resonant inverter controlled by frequency modulation-pulse density modulation-based fuzzy logic controller for induction heating system

Salih Nacar *

Faculty of Engineering and Natural Sciences, Department of Electrical Engineering, Bandırma Onyedi Eylül University, Balıkesir, TÜrkiye.

* Corresponding author: snacar@bandirma.edu.tr (S. Nacar)

Received 4 September 2022; Received in revised form 23 October 2023; Accepted 21 November 2023

Keywords

Class-E inverter;
Induction heating;
Soft switching;
Fuzzy Logic Controller (FLC);
Hybrid control;
Frequency Modulation (FM);
Pulse Density Modulation (PDM).

Abstract

The metal hydride tube used to store the hydrogen needs to be heated to remove the moisture inside and allow the hydrogen to flow out in it. Instead of conventional heating methods, the induction heating method is used to heat the metal hydride tube in this study. Class-E inverter constitutes the power stage of the system because of its simple structure, easy applicability, and low cost. The power switch of the inverter is driven with hybrid control, in which Frequency Modulation (FM) and Pulse Density Modulation (PDM) techniques are used together. Thus, the situations where one of the techniques is more advantageous than the other are utilized. Moreover, the positive aspects of each technique are highlighted. Fuzzy Logic Controller (FLC), which is independent of changing system parameters, carries out the power control of the inverter. A prototype of 232 W system consisting of the power and control circuit is established to verify the theoretical analysis and functionality of the hybrid control. To fix the tube temperature to the reference temperature of 250°C, the system is controlled in a closed-loop with FM-PDM-based FLC in the switching frequency range of 25-35 kHz. Highly efficient power control is carried out with FM-PDM-based FLC in a wide range.

1. Introduction

Induction heating has many advantages over traditional heating methods, such as being fast, more efficient, heating only the workpiece, and no combustion waste. For this reason, it is used in many applications, from cooking to melting [1-4]. One of these applications is the heating carried out to remove the moisture in the metal hydride tube used for hydrogen storage and discharge the hydrogen stored in it [5]. Depending on the type of application and output power required for induction heating, the high-frequency alternating current is produced with a single switch or half/full-bridge inverter topologies [6-9]. Class-E inverters are preferred due to their simple structure, ease of application, and low cost in applications up to 3 kW [10,11]. Unlike the study [5], class-E inverter is used in the power stage of the induction heating system when the advantages of class-E inverter and the amount of power required for the application are considered. In addition, in this study, the system's prototype is realized, and the induction heating method is used to heat the tube, unlike in the studies [12,13]. Although class-E inverter has different topologies [14-17], the circuit topology used in the study [17] is preferred for induction heating applications. The reasons for the preference of the topology are that there is no need for an additional element for the resonance circuit since the work coil is used directly as a resonant element, and the power switch connected directly to the ground is easy to drive [14,17].

Another issue as significant as the inverter topology to be used in induction heating applications is the determination of the techniques used in the control of the inverter switch(s).

To cite this article:

S. Nacar "Design and implementation of class-E resonant inverter controlled by FM-PDM-based FLC for induction heating system", *Scientia Iranica* (2025) **32**(10): 7129. https://doi.org/10.24200/sci.2023.61067.7129

The techniques affect the operating frequency of the inverter, operating under soft-switching conditions, power regulation, output response speed, efficiency, and the operating voltage/current of the power switch(s) [18]. Different techniques such as phase-shift [19], duty cycle [20], Frequency Modulation (FM) [14] and Pulse Density Modulation (PDM) [21] are used to drive the power switch of class-E inverter. Phase-shift control is used for the power control of two identical class-E inverters connected in parallel. With this technique, the output power is precisely controlled by adjusting the phase difference between the two inverters against load changes. However, the requirement for two identical inverters connected in parallel to apply the phase-shift technique restricts its use in a single-stage class-E inverter [19]. In duty cycle control, the output power of the inverter is controlled practically by changing the duty ratio of the power switch. However, the fact that the switch has a limit value for the duty ratio at which it can operate under Zero Voltage Switching (ZVS) conditions prevents power control from being carried out over a wide range under ZVS conditions [20]. Although phase-shift and duty cycle techniques are employed in controlling class-E inverters, FM [14,22,23] and PDM [21, 24-26] techniques are commonly used for controlling preferred structure in induction heating applications. The advantages of FM are its simple structure and easy applicability. However, the disadvantages are increasing switching losses with increasing switching frequency, providing soft-switching conditions within certain limits, the power control in a narrow frequency range, and constantly updating the duty ratio. The advantages of PDM are that it operates at a fixed switching frequency and performs power control over a wide range. However, the disadvantages are that its implementation is difficult due to its complex structure and the power resolution depends on the frequency of the control signal. Also, audible noises occur when the frequency of the control signal is selected in the range of 20 Hz to 20 kHz, and the switch current and voltage stresses are high in the first period of the duty ratio of each new PDM signal, according to steady-state conditions [18,27].

In this study, instead of using one of the phase-shift [19], duty cycle [20], FM [14], or PDM [21] techniques for controlling the E-class inverter, which forms the power stage of the induction heating system, the hybrid control technique in which two of these techniques are used together is proposed. The FM and PDM techniques, commonly employed in induction heating applications [14, 21-26], are preferred techniques for hybrid control. Considering the specified advantages and disadvantages of the FM and PDM techniques [17,18,24], the control of the inverter is performed using the hybrid method that utilizes the favorable aspects of both, and it is tested in the induction heating system. In the study, firstly, the inverter is analyzed, and the maximum switching frequency values at which the power switch can operate under ZVS conditions are determined for different Quality factor (Q) values. Considering these frequency values, the power switch's maximum operating voltage and current values are obtained according to frequency. Moreover, according to these data, the switching frequency range in which the inverter can operate under ZVS conditions and other operating parameters are determined, and its design is carried out. As soon as the system is started, the control of the inverter's power switch is carried out by FM in the switching frequency range where ZVS conditions are guaranteed. In the FM technique, unlike PDM, the steady-state conditions are not disrupted at regular intervals, thus preventing the increase in the current and voltage stresses of the switch. When the maximum value of the switching frequency range determined in the control of the power switch with FM is reached and the output power of the inverter is desired to be further reduced, the switching frequency is fixed to the maximum value, and PDM is activated to control the power switch. Since the switching frequency of the PDM control is the maximum switching frequency value at which ZVS conditions are guaranteed, the increases in the switch current and voltage stresses that occur in the first period of the duty ratio of the PDM control signal are limited. In addition, the inverter's low output power values, which cannot be controlled by FM under ZVS conditions, can be controlled with high resolution up to 0 W using PDM. Thus, the temperature of the workpiece closely follows the reference temperature, without the ZVS conditions of the power switch disappeared.

In induction heating systems, the load parameters are constantly changing under different operating conditions [28]. The power control of such systems, which are non-linear and difficult to express mathematically, is very difficult with traditional Proportional Integral Differential (PID) control. However, Fuzzy Logic Controller (FLC) is effectively used in the control of systems with non-linear loads such as battery charging, electrolysis, induction heating, and maximum power point tracking [29-32]. Moreover, FLC is more robust than PID in the power regulation against changing system parameters such as input voltage, load, and reference value [30]. Due to its stated advantages, the power control of the inverter is carried out with FLC so that the workpiece temperature follows the reference value.

2. Hybrid controlled class-E resonant inverter for induction heating

The circuit structure of the induction heating system is as given in Figure 1. The system generally consists of the power and control circuit. The power circuit ZVS class-E inverter consists of the loaded heating coil, power switch, and resonant capacitor *C*. The input energy source of the inverter is the DC V source. While the Metal Oxide Semiconductor Field-Effect Transistor (MOSFET) *M* is used as the switch in the power circuit, the diode *D* is the body diode of *M*. The Digital Signal Controller (DSC) dspic33fj16gs502 with

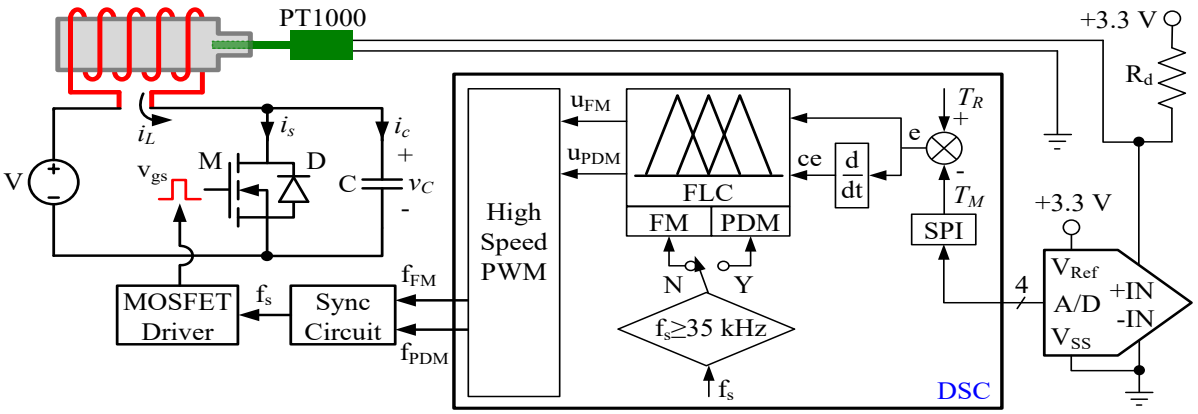

Figure 1. Induction heating system.

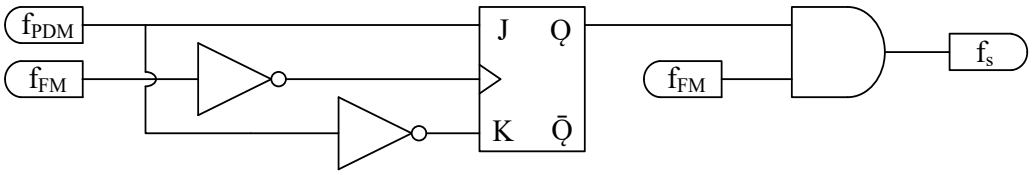

Figure 2. The synchronization circuit.

a high-speed Pulse Width Modulation (PWM) module is used to drive FM-PDM-based FLC, to obtain the switching signal of FM and the control signal of PDM.

The workpiece temperature, which is the feedback of the control circuit, is sensed by the PT1000 and then converted to a voltage by the voltage divider. T_M is obtained by digitizing this voltage with 12-bit A/D. The inputs of FLC are the error and derivative of the error. The error (e) is the difference between the reference temperature T_R and T_M. To decide to operate FLC for which control technique, a comparison is made as to whether the switching frequency (f_s) is higher than 35 kHz. If the comparison result is correct, FLC is run based on PDM, but otherwise, it is run based on FM. For the frequency values at which FLC operates based on FM, the duty ratio of the control signal (f_{PDM}) of the PDM is 100%. While u_{FM} is the change in the switching period, u_{PDM} is the change in the duty ratio of the control signal of PDM. By applying u_{FM} and u_{PDM} to dspic's high-speed PWM module, the PWM signal (f_{FM}) and the control signal of PDM (f_{PDM}) are generated, respectively. The synchronization circuit, shown in Figure 2 and consisting of JK flip-flop, NOT gates, and AND gate, is used to enable the simultaneous operation of f_{FM} and f_{PDM}.

The output (f_s) of the synchronization circuit is applied to the MOSFET driver circuit and the gate signal (v_{gs}) of the MOSFET is obtained.

2.1. ZVS class-E inverter

The equivalent circuit of the power circuit ZVS E-class resonant inverter is given in Figure 3.

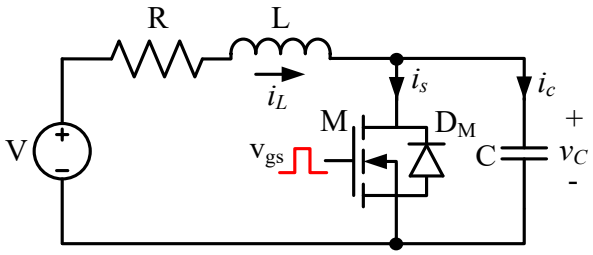

Figure 3. The equivalent circuit.

As can be seen from the equivalent circuit in Figure 3, the heating coil and the workpiece are represented by equivalent coil L and equivalent resistance R. When accepted that the circuit operates in steady-state conditions and all circuit elements are ideal, the values of L and C largely determine the operation and characteristics of the inverter. In this case, the following variables can be defined depending on the resonance parameters [17,33,34].

$$\omega_0 = \frac{1}{\sqrt{LC}}, \tag{1}$$

$$\omega = \sqrt{\frac{1}{LC} - \left(\frac{R}{2L}\right)^2}, \tag{2}$$

$$Z_0 = \sqrt{\frac{L}{C}}, \tag{3}$$

$$Q = \frac{\omega_0 L}{R}, \tag{4}$$

$$\alpha = \frac{R}{2L}. \tag{5}$$

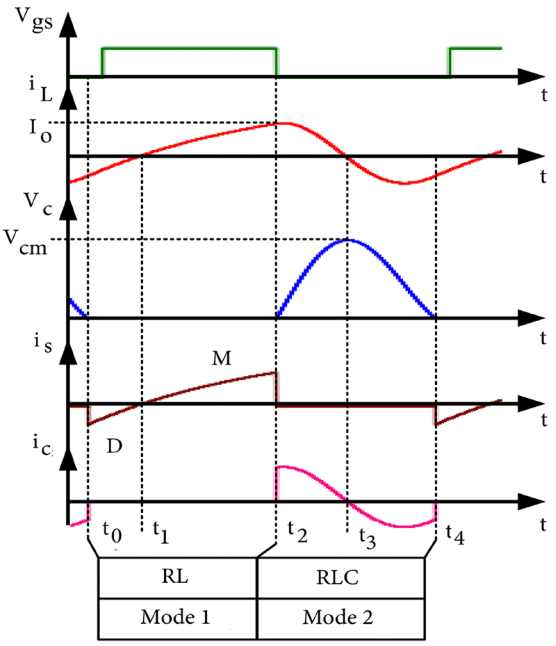

Figure 4. The waveforms of the inverter.

In the given equations, the resonance angular frequency ω_0, the damped angular frequency ω_0, the characteristic impedance Z_0, the quality factor Q, and the neper frequency α. Considering the states of the power switch M and diode D_M and the transient response of the resonant circuit for steady-state conditions, four different operating intervals occur for a switching period. The waveforms of the gate signal (v_{gs}), coil current (i_L), capacitor voltage (v_c), switch current (i_s), and capacitor current (i_c) for these time intervals are given in Figure 4.

Although the inverter has four different operating intervals, two different operating states, RL and RLC, occur depending on whether the power switch and diode are turned on or off. These circuit structures are series RL for the case where switch M or D_M is turned on (Mode 1), and the series RLC circuit for the case where both switches are turned off (Mode 2).

Assuming that the inverter operates in steady-state conditions and all circuit elements are ideal, the operation of the inverter for Mode 1 and Mode 2 is as follows:

Mode 1 ***($t_0 \le t < t_2$):*** When the capacitor voltage is 0 V at the time t_0, D_M diode is turned on and carries the negative current i_L in the series RL circuit whose initial value is I_{Lt0}. For the M switch clamped to the diode voltage, the ZVS conditions are met from the moment t_0 to the moment t_1 when i_L reaches 0 A. At the time t_2, when the duty rate of v_{gs} ends, L is charged to the value of I_o. The equality of i_L is as given in Eq. (6). τ in Eq. (6) is the time constant of the series RL circuit and is L/R.

$$i_{L(t)} = \frac{V}{R}(1 - e^{-\frac{t}{\tau}}) + I_{Lt0}e^{-\frac{t}{\tau}}. \tag{6}$$

Mode 2 ***($t_2 \le t < t_4$):*** At the moment of t_2, when switch M is turned off, the series RLC circuit is formed, and the oscillation between L and C begins. The phase-plane, which converts resonant waveforms into simple geometric shapes, can be used to determine the oscillation conditions and limits of the series RLC circuit with an initial current of I_o. The phase-plane curve of the inverter is given in Figure 5 [33].

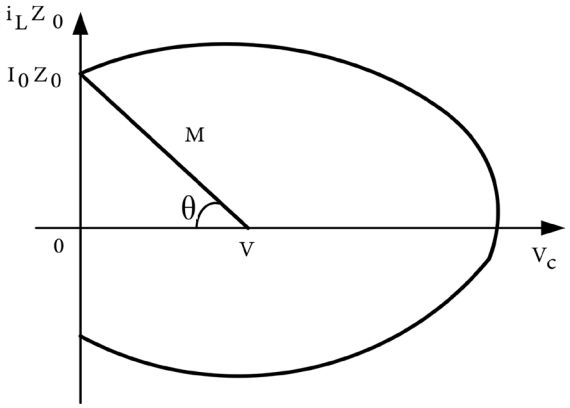

Figure 5. The phase-plane curve.

In the phase-plane curve, M is the absolute value and θ is the phase angle. M and θ are as given in Eqs. (7) and (8), respectively.

$$M = \sqrt{I_o^2 \frac{L}{C} + V^2}, \tag{7}$$

$$\theta = \tan^{-1}\left(\frac{I_o Z_0}{V}\right), \tag{8}$$

while the capacitor C, whose voltage value is 0 V at the time of t_2, is charged to the value of V_{cm} at the time t_3, the coil current i_L becomes 0 A. The oscillation between L and C continues until the capacitor voltage is 0 V. The equations of i_L and v_c for this time interval are given in Eq. (9) and Eq. (10), respectively [17].

$$i_{L(t)} = \frac{M}{Z_0}e^{-\alpha t}\sin(\omega t + \theta), \tag{9}$$

$$v_{c(t)} = V - Me^{-\alpha t}\cos(\omega t + \theta). \tag{10}$$

The damping ratio of the curve starting at t_2 and continuing in a spiral until t_4 is as given in Eq. (11).

$$\delta = \frac{\alpha}{\omega_0} = \frac{1}{2Q}. \tag{11}$$

In interval Mode 2, the phase-plane curve passes through the maximum value of the coil current and capacitor voltage. The maximum coil current I_{Lm} ($\omega t = (\pi/2) - \theta$) and the maximum capacitor voltage V_{cm} ($\omega t = \pi - \theta$) can be found in Eq. (12) and Eq. (13), respectively.

$$I_{LM} = \frac{M}{Z_0}e^{-\left(\frac{\frac{\pi}{2}-\theta}{2Q}\right)}, \tag{12}$$

$$V_{cm} = V + Me^{-\left(\frac{\pi-\theta}{2Q}\right)}. \tag{13}$$

While the capacitor voltage v_c reaches 0 V at time t_4 ($\omega t = 2\pi - \theta$), i_L continues to oscillate. While v_c drops to 0 V, the limit condition for oscillation given in Eq. (14) should be satisfied for the diode D_M to be turned on and the ZVS conditions of switch M to occur.

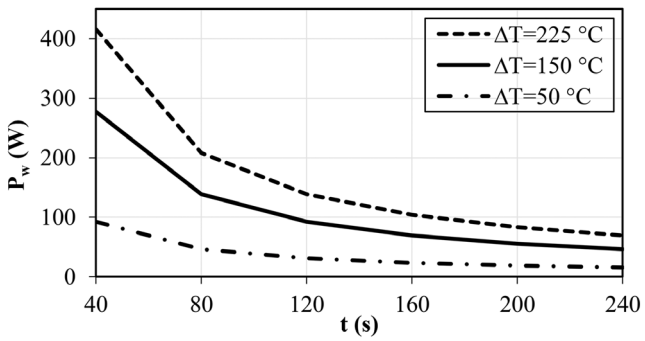

Figure 6. The power-time graph for different temperature changes.

$$V = Me^{-(\frac{2\pi-\theta}{2Q})}. \quad (14)$$

For Mode 1 and Mode 2, while the operating of the inverter is completed at time t_4, the operation starts again from t_0 and similarly continues until t_4.

2.2. *Design of the inverter*

The power equation given in Eq. (15) determines the operating power of the inverter used in the induction heating system. In the equation, m is the mass (kg) of the workpiece, and c (specific heat) is the quantity (J/kg°C) of thermal energy absorbed by one gram of the workpiece to raise the temperature of the workpiece by one degree Celsius. T_f and T_i are the final and initial temperatures of the workpiece, respectively. Finally, t is the time (s) required to reach the final temperature [35].

$$P_w = mc\frac{T_f - T_i}{t}. \quad (15)$$

The power-time graph for different temperature changes ($\Delta T = T_f - T_i$) of the metal hydride tube made of steel st52 (carbon steel) material with the specific heat of 490 J/kg°C and the mass of 0.151 kg is given in Figure 6. As seen in Figure 6, while the power value required to obtain high-temperature differences on the workpiece in a short time increases, the power value decreases in the opposite case.

The time taken to heat the tube from room temperature of 25°C to the reference temperature of 250°C is chosen as 90 s. For a temperature difference of 225°C to occur in the tube in 90 s, the power value (P_w) that must be transferred to the tube is found by Eq. 15 as 185 W. Assuming the inverter efficiency is 0.8, the average power (P_0) to be supplied by the source is 231.25 W. In Figure 7, the heating coil designed by considering the physical properties of the tube and the tube itself are given. The heating coil is implemented using insulated 0.35 mm Litz wire to reduce the skin effect. As a result of the experimental studies, the equivalent inductance L and equivalent resistance R parameters of the loaded heating coil for the workpiece temperature of 250°C are determined as 82.13 µH and 2.6 Ω, respectively.

To determine the Q value of the inverter, considering the oscillation condition where the soft-switching condition is satisfied, V_{cm} and I_{Lm} curves according to the normalized

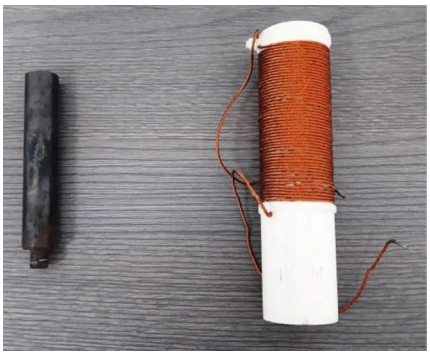

Figure 7. The tube and heating coil.

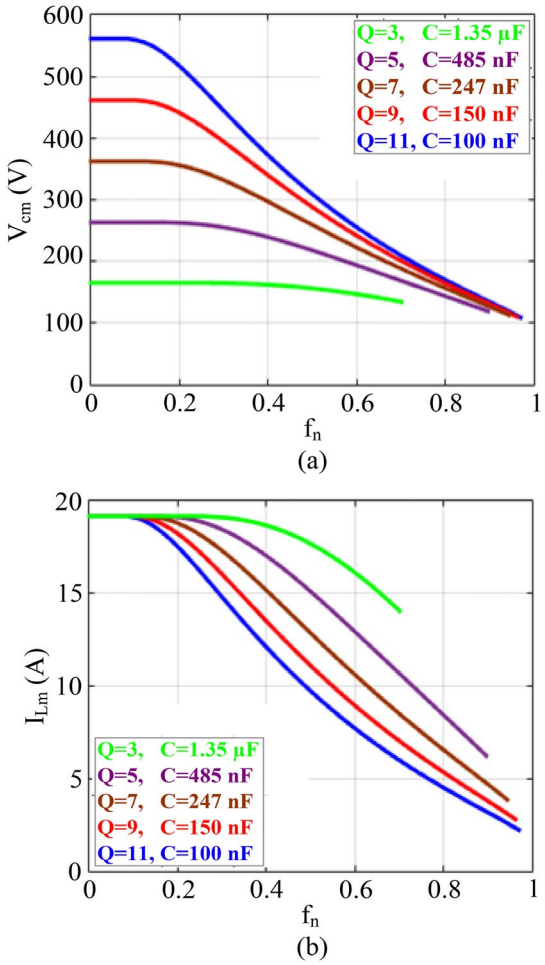

Figure 8. f_n-V_{cm} and f_n-I_{Lm} curves for different Q value, (a) f_n-V_{cm}, and (b) f_n-I_{Lm}.

frequency for different Q values are obtained and given in Figure 8. Since the value of L, one of the resonant elements of the inverter, is known, the C value obtained for each different Q value is also given in Figure 8.

As seen in Figure 8, while the switch voltage V_{cm} increases with increasing Q value, the maximum current I_{Lm} carried by the switch decreases. Therefore, the value of Q determines the voltage and current stress of the switch. Moreover, since the capacitance value of the capacitor increases with decreasing Q value, the resonance frequency also decreases and the switching frequency, which is the control variable, reduces to the audible frequency values. In

Table 1. The operating parameters of the inverter.

V (V)	L (μH)	C (nF)	R (Ω)	f_r (kHz)	P_0 (W)
50	82.13	150	2.6	45.34	231.25

addition to considering these factors in determining the Q value, the low switch voltage facilitates the selection of the switch. Also, due to the low voltage level that the switch is exposed to, insulation losses are reduced, and transmission resistance, which increases with the operating voltage of power switches such as Insulated Gate Bipolar Transistor (IGBT), is prevented. However, the current (I_{Lm}) carried by the switch increases for the low switch voltage. Considering all these factors, the quality factor of the inverter is chosen as 9. With the determination of the Q value, the operating parameters of the inverter are given in Table 1.

For the determined Q value, when the minimum switching frequency of the inverter is accepted as 20 kHz, which is the audible frequency, the maximum switch voltage and current are 330 V and 12.5A, respectively. MOSFET, which is more suitable for ZVS because the turned-on losses are higher than the turned-off losses, is preferred as the power switch in the inverter. In addition, the determined maximum switch voltage and current values are suitable for using MOSFET as the power switch. For this reason, MOSFET IRFP460 with a maximum operating voltage and current of 500 V and 20 A, respectively, is preferred as the power switch.

2.3. Control of the inverter

Eq. (16), from which the average power produced by the source is calculated, is used to determine the frequency range at which the inverter power control will be performed.

$$P_0 = Vf_s \int_{t_1}^{t_2} i_{L(t)} dt. \tag{16}$$

Considering the limit condition for the oscillation for the determined Q, the curve of the average power produced by the source according to the normalized frequency is given in Figure 9. As can be seen from Figure 9, while the average power of 231.5 W is generated by the source at the switching frequency of 25.01 kHz, the minimum average power of 22 W is generated at the switching frequency of 42.61 kHz.

To reduce the average power below 22 W in the FM-controlled inverter, the switching frequency must be increased. However, as can be seen from Figure 10, which shows the variation of the capacitor voltage with the frequency for Mode 2, the limit condition for oscillation cannot be met for the frequency value above the switching frequency of 42.64 kHz. Therefore, the voltage v_c, which should be 0 V at the end of the Mode 2 interval, continues to oscillate without falling to 0 V. As a result, since the power switch cannot be turned on under the ZVS condition, the switching losses increase, and the efficiency decreases.

As a result of the analyses, the minimum operating frequency, where the power required to create the temperature

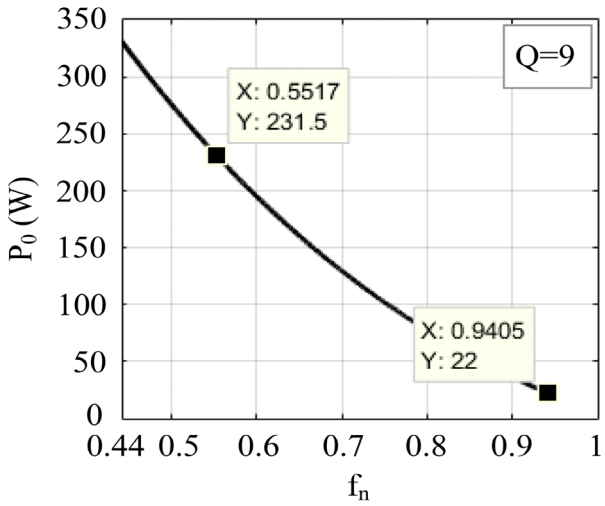

Figure 9. P_0-f_n curve.

Table 2. Rule base.

e/ce		ce				
		NB	**NS**	**Z**	**PS**	**PB**
e	NB	NB	NB	NB	NB	Z
	NS	NB	NS	NS	Z	PB
	Z	NB	NS	Z	PS	PB
	PS	NB	Z	PS	PS	PB
	PB	Z	PB	PB	PB	PB

temperature difference on the workpiece in the desired time is obtained, is determined as 25.01 kHz. The maximum operating frequency is selected as 35 kHz, and the power control of the inverter is performed with FM in this range. Thus, the ZVS conditions of the power switch are guaranteed. However, the average power produced by the source for the 35 kHz switching frequency is 91.13 W. To control the power of the inverter from 91.13 W to 0 W, the switching frequency is fixed at 35 kHz and PDM control is activated. The power-frequency curve of the hybrid control, whose working principle is explained, is given in Figure 11.

As seen in Figure 11, the control of the inverter is carried out with FM for high powers and with PDM for medium and low powers. With the hybrid method in which FM and PDM are used together, the power of the inverter is controlled up to 0 W while maintaining the ZVS conditions.

2.4. Power control of the inverter with FM-PDM-Based FLC

In the induction heating system controlled by FLC, the regulated output magnitude is the temperature of the workpiece. There is no need for a mathematical model to control the induction heating system with FLC. Instead, the expert knowledge and the operation of FLC units (fuzzification, rule base, inference engine, and defuzzification) within the framework of definite rules are sufficient for control of the system. The rule base of FLC is given in Table 2. The input and output linguistic variables N, S, Z, P, and B of FLC are negative, small, zero, positive, and big, respectively. The rule base of FLC is built with IF-THEN rules.

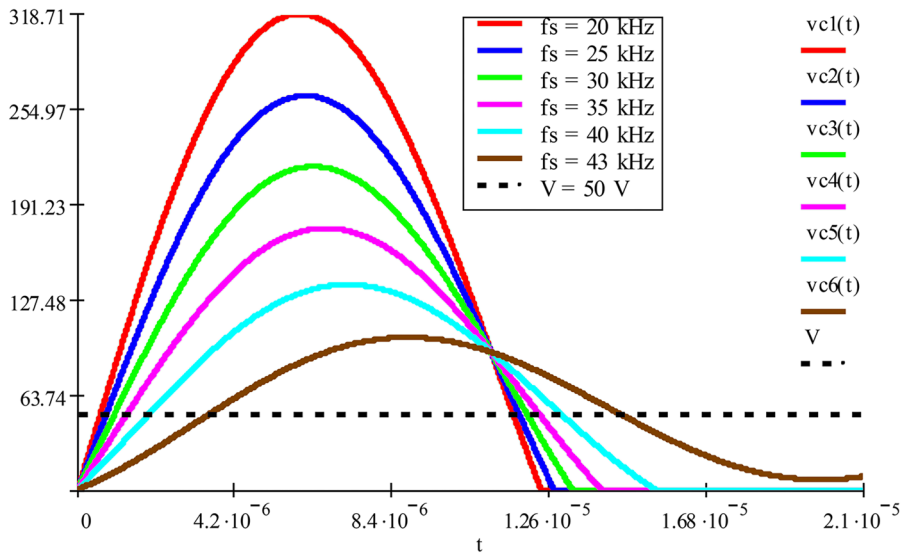

Figure 10. Variation of the capacitor voltage with the frequency for Mode 2.

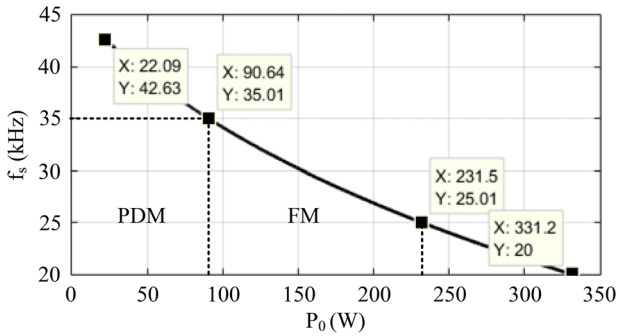

Figure 11. The power-frequency curve of the hybrid control.

Membership functions of FM-PDM-based FLC are given in Figure 12. Triangle and trapezoid are used as membership functions in input (e and ce) and output (u) variables of FLC. In the membership graphs in Figure 12, while the *x*-axis shows the membership values of the variables, the *y*-axis (μ) shows the membership degree of the relevant variable. Min-max (Mamdani) is used as the fuzzy inference method and the centre of gravity is used as the defuzzification method in FLC. Membership functions of FLC are selected the same for FM and PDM control. While the limit values of the input membership functions for FM and PDM are equal, the limit values for the output membership functions are different. When the switching frequency reaches 35 kHz, the power control of the inverter is switched from FM control to PDM control technique, and the limit values of the output membership functions are updated.

Thus, thanks to the FM-PDM-based FLC structure, the power control of the inverter is realized by using two different switch driving techniques together.

3. Experimental studies

The experimental setup of the induction heating system with the FM-PDM-based FLC controlled class-E inverter is given in Figure 13(a) and, the inverter and control circuit are given in Figure 13(b). The system is operated with the input voltage V, which is obtained by DC power supply. TC4427 driver integrated circuit is used to drive the MOSFET IRFP460. To provide a high coupling factor between the heating coil and workpiece, the heating coil is designed depending on the physical properties of the metal hydride tube. The heating coil is wound in 53 turns. In experimental studies, the coil current is measured with Tektronix 011-0105-00 AC current probe. Polypropylene capacitor, developed for energy conversion and control in power electronics applications, is used as the resonance capacitor. To detect the workpiece temperature, which is the system's feedback, the two-end PT1000 resistance temperature detector, which can measure temperature from -200°C to 400°C, is used. 12-Bit A/D converter MCP3204 integrated circuit is used to digitize the temperature information from the PT1000 by communicating with the DSC through a simple serial peripheral interface. In addition, for faster analog-to-digital conversion and more accurate measurement, the supply voltage, and the reference voltage of MCP3204 are selected to be 5 V and 3.3 V respectively. The temperature is also sensed with a K-type thermocouple and transferred to the computer environment with the TC-08 data logger to display the temperature-time variation of the metal tube.

To verify the validity of the analysed and designed inverter, when the temperature of the workpiece is 250°C, the gate signal of the power switch, coil current, and capacitor voltage waveforms for different frequency values are given in Figure 14. ZVS conditions are satisfied for the power switch from 25 kHz to 40 kHz. In addition, from the measurements carried out at approximately 5 kHz intervals

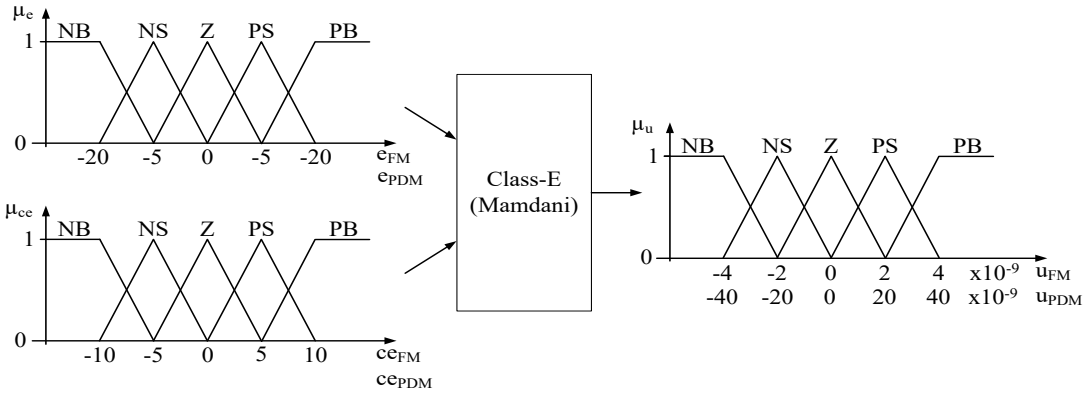

Figure 12. Membership functions of FM-PDM-based FLC.

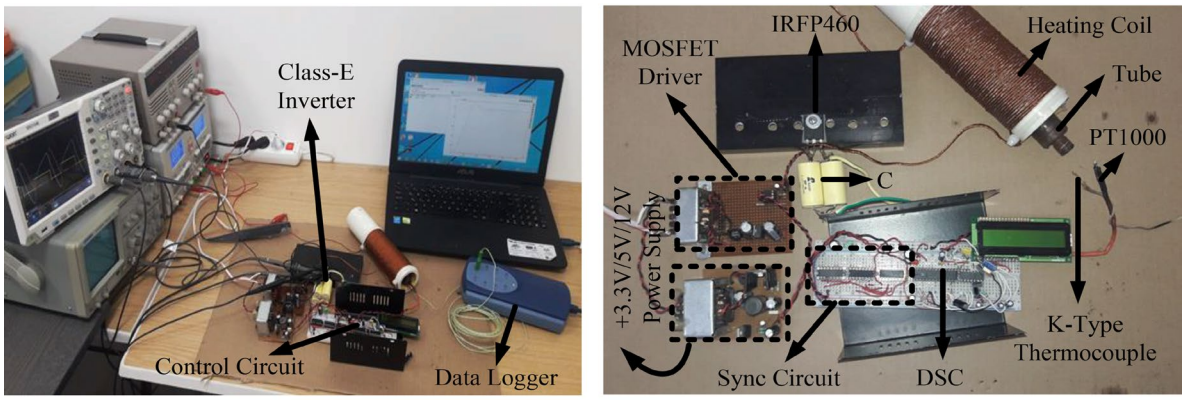

(a) (b)

Figure 13. The induction heating system: (a) The experimental setup; and (b) the inverter and control circuit.

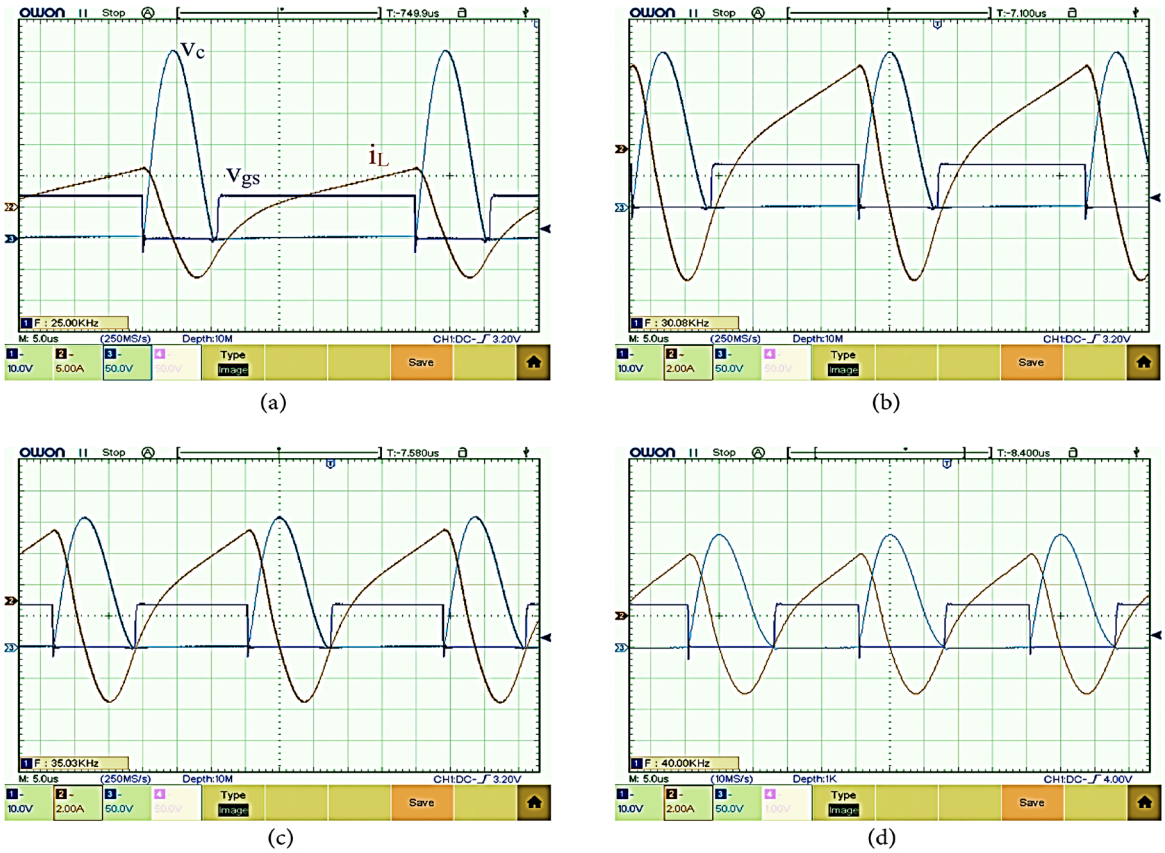

(a) (b) (c) (d)

Figure 14. The gate signal of the power switch, coil current, and capacitor voltage waveforms for different frequency values: (a) 25 kHz; (b) 30 kHz; (c) 35 kHz; and (d) 40 kHz.

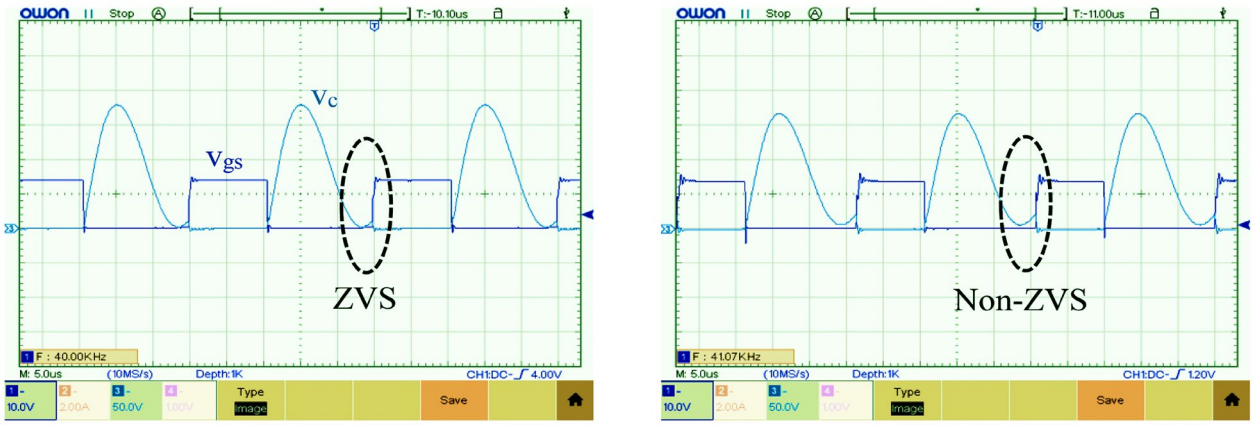

Figure 15. The states of ZVS for the different frequencies: (a) 40 kHz; and (b) 41.07 kHz.

from 25 kHz to 40 kHz, it is seen that the peak values of coil current (i_L) and capacitor voltage (v_c) support each other with the theoretical analysis (see Figure 8) for the determined quality factor ($Q = 9$).

From the gate signal and capacitor voltage given in Figure 15(a), it is seen that v_c voltage drops to 0 V for 40 kHz switching frequency, and ZVS conditions are satisfied. However, from Figure 15(b), it is seen that v_c does not drop to 0 V with the increase of switching frequency as of 41.07 kHz, and ZVS conditions are not satisfied.

The system is operated in the open loop for the minimum switching frequency (25 kHz) while the workpiece temperature is 25°C. The system is started in 30th second and the workpiece temperature reaches 250°C in 122nd second. As a result, it is seen that the time determined for the formation of the temperature difference of 225°C on the workpiece during the design of the inverter and the time observed as a result of the experimental studies are very close to each other. The temperature difference of 225°C on the workpiece occurs in 92 seconds.

The temperature-time graph of the workpiece for this operating state is given in Figure 16.

To compare the maximum values of the switch voltage and coil current for FM and PDM techniques, the power control of the inverter is carried out with PDM when the workpiece temperature is 250°C. The gate signal, coil current, and capacitor voltage waveforms of the PDM controlled inverter are given in Figure 17 for the different switching frequencies and duty ratios.

The switch voltage and coil current peak values for the same operating parameters of FM and PDM controlled inverters are given in Table 3. The peak value of the switch voltage and coil current in the first period of the PDM switching signal is higher than that of the FM-controlled inverter because there are no steady-state conditions at the beginning of each PDM period in the PDM controlled inverter.

The induction heating system is controlled in a closed-loop with FM-PDM-based FLC in order that the temperature of the workpiece follows the reference temperature of 250°C with the hybrid-controlled inverter. The temperature-time graph of the workpiece, which is the response of the system, is given in Figure 18.

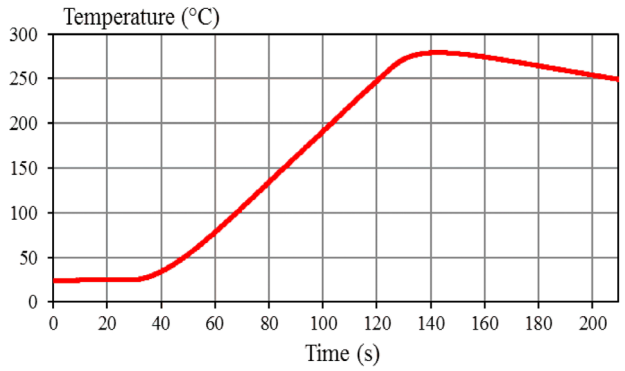

Figure 16. Temperature-time graph of the workpiece for the fixed operating frequency of 25 kHz.

While the workpiece temperature is 26°C, the system starts at 26th second, and the workpiece temperature reaches the set point in approximately 120 seconds. The maximum value of the workpiece temperature is 272°C and the settling time is approximately 161 seconds. To show that the FM-PDM-based FLC used in the power control of the inverter performs its function correctly, the gate signal, coil current, and capacitor voltage of the inverter are measured at different temperature and time values of the curve in Figure 18. The measurement results are given in Figure 19.

As seen in Figure 19(a), while the workpiece temperature is 56°C at 50th second, the operating frequency of the inverter is 25 kHz, and the power switch is driven by FM control. While the workpiece temperature is 223°C at 110th second, it is seen from the waveforms in Figure 19(b) that the operating frequency of the inverter is 32.52 kHz, and FM-based operation continues. In Figure 19(c) given for the 124th second and the workpiece temperature of 261°C, PDM-based operation is started, and the operating frequency is fixed at 35 kHz.

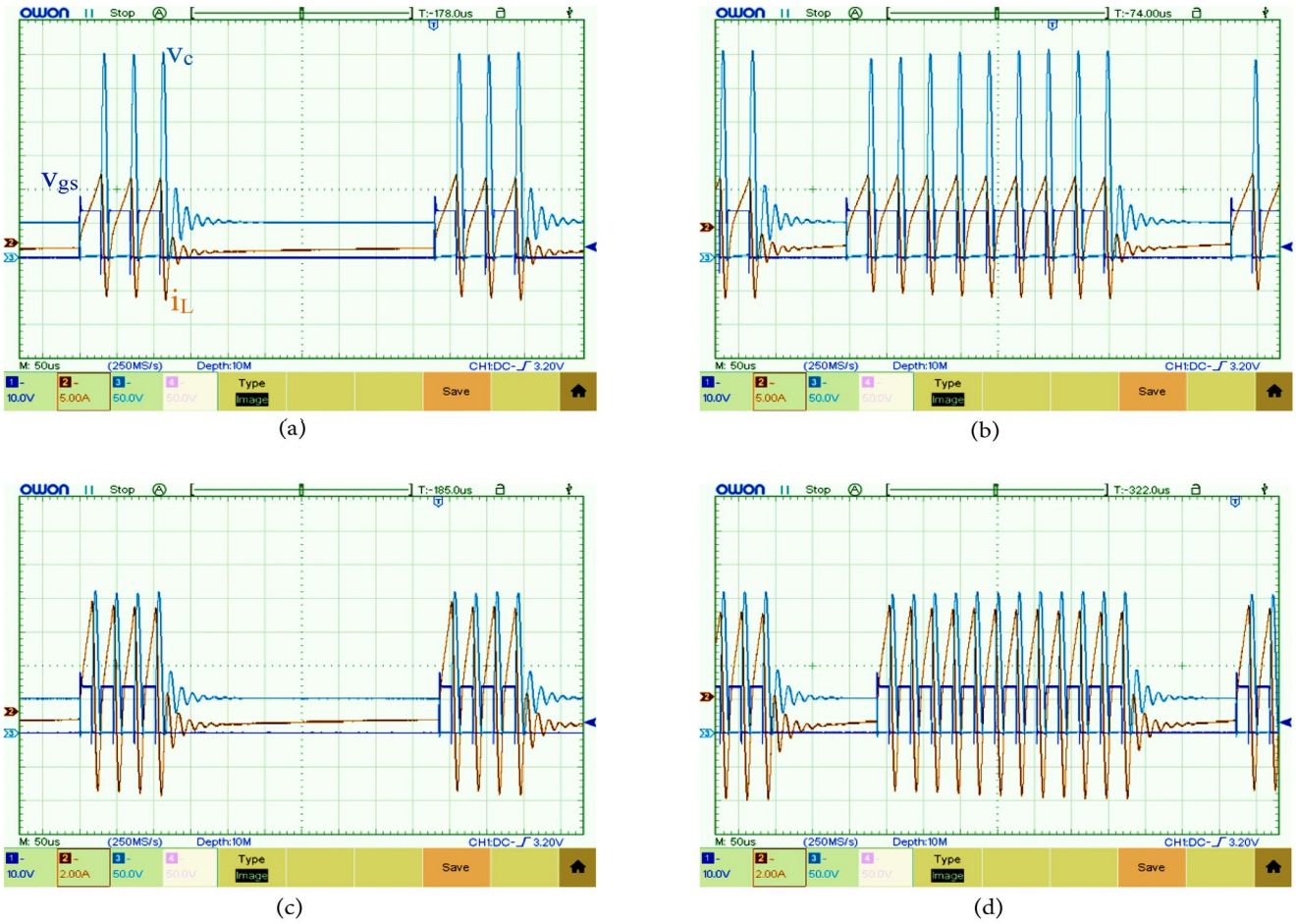

Figure 17. The gate signal, coil current, and capacitor voltage waveforms of the PDM controlled inverter: (a) f_s=25 kHz and D=%25; (b) f_s=25 kHz and D=%75; (c) f_s=35 kHz and D=%2; and (d) f_s=35 kHz and D=%75.

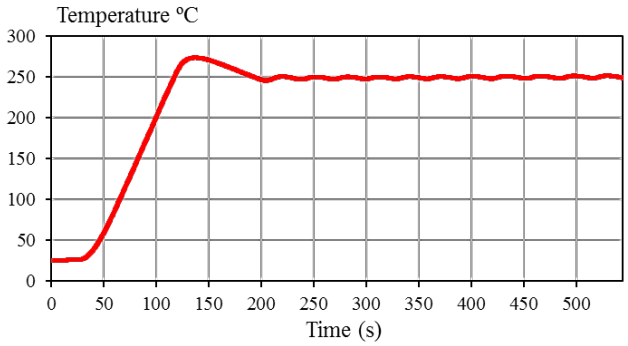

Figure 18. The response of the closed loop system.

Table 3. The switch voltage and coil current peak values of FM and PDM controlled inverter.

Control	f_s (kHz)	V_{cm} (V)	I_{Lm} (A)
FM	25	300	10.9
PDM	25	310	12.5
FM	35	210	7.5
PDM	35	220	7.9

From Figure 19(d) given for 225th second and the workpiece temperature of 251°C, it is seen that PDM-based operation continues with the fixed 35 kHz switching frequency. According to the temperature-time graph given in Figure 18 and the measurement results given in Figure 19, FM-PDM-based FLC operates in accordance with its purpose and follows the reference temperature value.

4. Conclusions

In the study, a closed-loop induction heating system is implemented to heat the metal hydride tube whose temperature to follow the reference temperature of 250°C. The class-E inverter used in the system's power stage has a high switch peak voltage but is simple in structure, low in cost, and especially suitable for low-power applications. First, the theoretical analysis of the inverter is carried out, then the parameters of the loaded heating coil are determined for the reference temperature of 250°C, and finally, the design of the inverter is carried out. The output power of the inverter, whose load parameters are constantly changing with the changing temperature, is controlled by Frequency Modulation and Pulse Density Modulation (FM-PDM)-based Fuzzy Logic Controller (FLC). The output power control is accomplished by Frequency Modulation (FM) with the switching frequency changing from 231.5 W to 90.64 W in the range of 25-35 kHz, and by PDM at the fixed switching

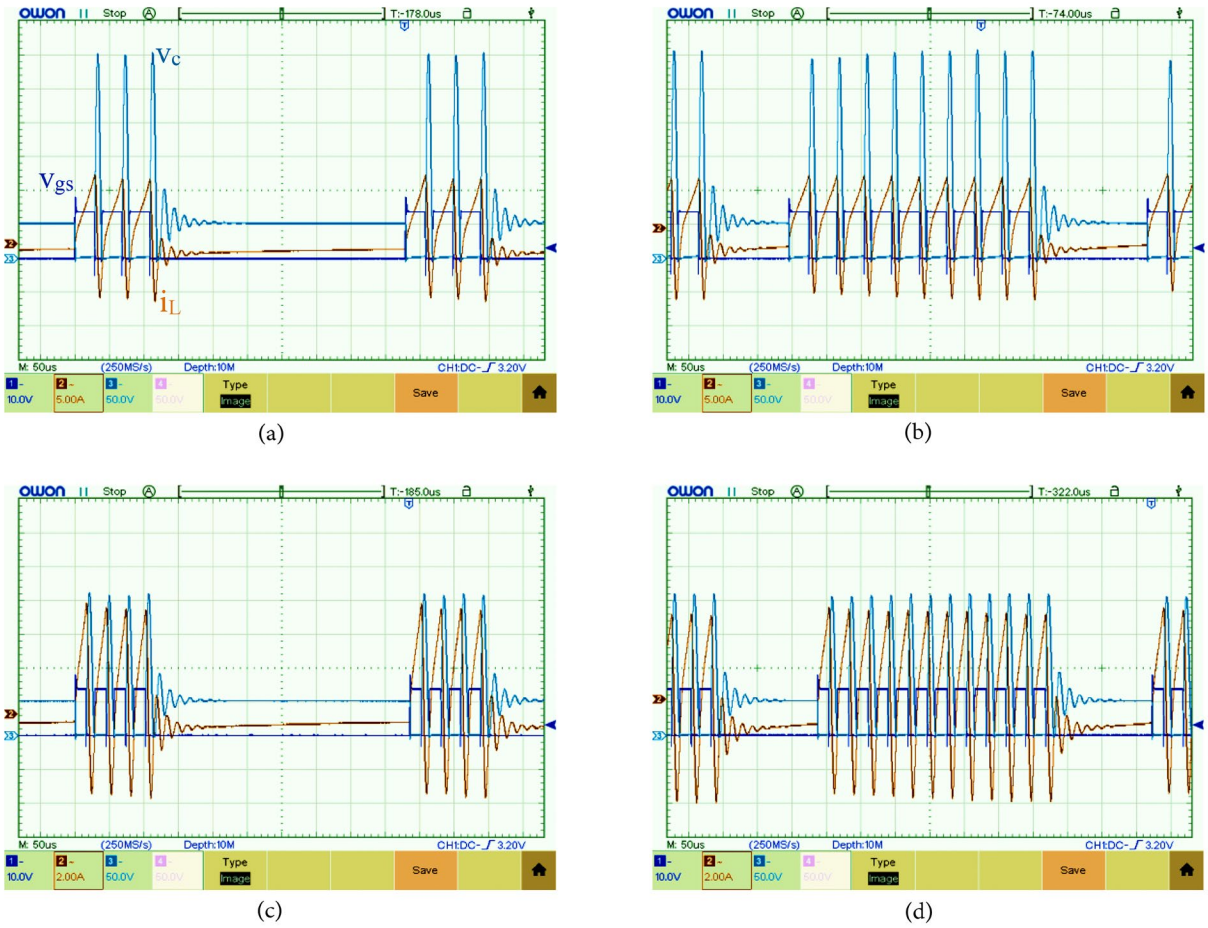

Figure 19. The waveforms of the gate signal, coil current and capacitor voltage at different temperature and time values of the curve in Figure 17: (a) For 50th second and 56°C; (b) for 110th second and 223°C; (c) for 124th second and 261°C; and (d) for 225th second and 251°C.

frequency of 35 kHz from 90.64 W to 0 W. In this way, while the ZVS conditions of the power switch are preserved from 0 W to 231.5 W, the power control of the inverter is performed by the hybrid method in which FM and PDM are used together. The theoretical analysis and design, as well as the functionality of the FM-PDM-based FLC control, are verified by the experimental studies on the prototype circuit. A low-cost microcontroller performs fully digital control of the system by executing the FM-PDM-based FLC control algorithm.

Acknowledgment

This research was supported by Bandırma Onyedi Eylül University Scientific Research Projects Unit (Project Number: BAP-21-1003-011).

Funding

This research did not receive any specific grant from funding agencies in the public, commercial, or not-for profit sectors.

Conflicts of interest

The authors declare that they have no known competing financial interests or personal relationships that could have appeared to influence the work reported in this paper.

Authors contribution statement

Author: Conceptualization; Data curation; Formal analysis; Investigation; Methodology; Project administration; Resources; Software; Supervision; Validation; Visualization; Roles/Writing-original draft; Writing-review and editing.

References

1. Hammouma, C. and Zeroug, H. “Enhanced frequency adaptation approaches for series resonant inverter control under workpiece permeability effect for induction hardening applications”, *Engineering Science and Technology, an International Journal*, **27**(2022), pp. 1-13 (2022). https://doi.org/10.1016/j.jestch.2021.05.010

2. Baranoğlu, B., Özbek, M.E., and Aydın, E. “Experimental analysis of an electromagnetic pulse forming systems pre-heated by induction”, *Journal of the Faculty of Engineering and Architecture of Gazi University*, **35**(4), pp. 2101-2112 (2020). https://doi.org/10.17341/gazimmfd.605773

3. Jang, E., Kwon, M.J., Park, S.M., et al. “Analysis and design of flexible-surface induction-heating cooktop with GaN-HEMT-based multiple inverter system”,

IEEE Transactions on Power Electronics, **37**(10), pp. 12865-12876 (2022). https://doi.org/10.1109/TPEL.2022.3175979

4. Kawashima, R., Mishima, T., and Ide, C. "Three-phase to single-phase multiresonant direct AC-AC converter for metal hardening high-frequency induction heating applications", *IEEE Transactions on Power Electronics*, **36**(1), pp. 639-653 (2021). https://doi.org/10.1109/TPEL.2020.3003026

5. Nacar, S. and Öncü, S. "Simulation of induction system used for hydrogen tube heating", *5. European Conference on Renewable Energy Systems*, ISBN: 978-605-86911-5-5, pp. 236-238 (2017).

6. Özbay, H., Karafil, A., and Öncü, S. "Sliding mode PLL-PDM controller for induction heating system", *Turk. J. Elec. Eng. & Comp. Sci*, **29**(2), pp. 1241-1258 (2021). https://doi.org/10.3906/elk-1908-62

7. Huang, M.S., Liao, C.C., Li, Z.F., et al. "Quantitative design and implementation of a cooker for a cooker for c copper pan", *IEEE Access*, **9**, pp. 5105-5118 (2021). https://doi.org/10.1109/ACCESS.2020.3046713

8. Züngör, F., Emre, B., Öz, B., et al. "A new load detection method and circuit analysis for quasi resonant inverter", *10th IEEE International Conference on Renewable Energy Research and Applications*, İstanbul, September 26-29, pp. 40-46 (2021). https://doi.org/10.1109/ICRERA52334.2021.9598568

9. Ozbay, H. "PDM-MPPT based solar powered induction heating system", *Engineering Science and Technology, an International Journal*, **23**(6), pp. 1397-1414 (2020). https://doi.org/10.1016/j.jestch.2020.06.005

10. Charoenwiangnuea, P., Wangnipparnto, S., and Tunyasrirut, S. "Design of a class-E direct AC-AC converter with only one capacitor and one inductor for domestic induction cooker", *18th International Conference on Electrical Engineering/Electronics, Computer, Telecommunications and Information Technology*, pp. 680-683 (2021). https://doi.org/10.1109/ECTICON51831.2021.9454917

11. Yeon, J.E., Cho, K.M., and Kim, H.J. "A 3.6 kW single-ended resonant inverter for induction heating applications", *17th European Conference on Power Electronics and Applications*, Geneva, 8-10 Sept., pp. 1-7 (2015). https://doi.org/10.1109/EPE.2015.7309110

12. Elhamshri, F.A.M. and Kayfeci, M. "Enchancement of hydrogen charging in metal hydride-based storage systems using heat pipe", *International Journal of Hydrogen Energy*, **44**(34), pp. 18927-18938 (2019). https://doi.org/10.1016/j.ijhydene.2018.10.040

13. Elhamshri, F.A.M., Kayfeci, M., Matik, U., et al. "Thermofluidynamic modelling of hydrogen absorption in metal hydride beds by using Multiphysics software", *International Journal of Hydrogen Energy*, **45**(60), pp. 34956-34971 (2020). https://doi.org/10.1016/j.ijhydene.2020.04.041

14. Komiyama, Y., Matsuhashi, S., Zhu, W., et al. "Frequency-modulation controlled load-independent class-E inverter", *IEEE Access*, **9**, pp. 144600-144613 (2021). https://doi.org/10.1109/ACCESS.2021.3121781

15. Charoenwiangnuea, P., Poungsri, P., Sriamad, K., et al. "An accurate time-domain waveforms of class-E ZVDS inverter in series- and parallel-load network for domestic induction cooker", *18th International Conference on Electrical Engineering/Electronics, Computer, Telecommunications and Information Technology*, Thailand, 19-22 May, pp. 1055-1058 (2021). https://doi.org/10.1109/ECTICON51831.2021.9454687

16. Lee, D.Y. and Hyun, D.S. "A new hybrid control scheme using active-clamped class-E inverter with induction heating jar for high power applications", *Journal of Power Electronics*, **2**(2), pp. 104-111 (2022). https://doi.org/10.1109/APEC.2002.989389

17. Sazak, B.S., Çetin, S., and Öncü, S. "A simplified procedure for the optimal design of induction cooking appliances", *International Journal of Electronics*, **94**(3), pp. 197-208 (2007). https://doi.org/10.1080/00207210601114867

18. Nacar, S., Öncü, S., and Bal, G. "Comparison of control techniques for series resonant converter", *GU J Sci*, **9**(2), pp. 283-296 (2021). https://doi.org/10.29109/gujsc.908600

19. Cheng, B. and He, L. "A double-pulse energy injection converter with reduced switching frequency for MHz WPT system", *IEEE Transactions on Microwave Theory and Techniques*, **69**(7), pp. 3475-3483 (2021). https://doi.org/10.1109/TMTT.2021.3076089

20. Li, YF., and Tseng, CS. "Tracking control of class-E inverter for the duty cycle control", *2014 IEEE 23rd International Symposium on Industrial Electronics (ISIE)*, Istanbul, 1-4 June, pp. 2643-2647 (2014). https://doi.org/10.1109/ISIE.2014.6865037

21. Karafil, A. "Thinned-out controlled IC MPPT algorithm for class-E resonant inverter with PV system", *Ain Shams Engineering Journal*, **14**(5), pp. 1-9 (2023). https://doi.org/10.1016/j.asej.2022.101992

22. Charoenwiangnuea, P., Ekkaravarodome, C., Boonyaroonate, I., et al. "Design of domestic induction cooker based on optimal operation class-E inverter with parallel load network under large-signal excitation", *Journal of Power Electronics*, **17**(4), pp. 892-904 (2017). https://doi.org/10.6113/JPE.2017.17.4.892

23. Park, N.J., Lee, D.Y., and Hyun, D.S. "Study on the new control scheme of class-E inverter for IH-jar application with clamped voltage characteristic using pulse

frequency modulation", *IET Electric Power Applications*, **1**(3), pp. 433-438 (2007). https://doi.org/10.1109/IAS.2002.1042732

24. Ekkaravarodome, C., Charoenwiangnuea, P., and Jirasereeamornkul, K. "The simple temperature control for induction cooker based on class-E resonant inverter", *10th International Conference on Electrical Engineering/Electronics, Computer, Telecommunications and Information Technology*, Thailand, 15-17 May, pp. 1-6 (2013). https://doi.org/10.1109/ECTICon.2013.6559634

25. Mungikar, H. and Jape, S. "Trends in energy conservation technology: temperature control of induction cooking applications using class-E resonant inverter", *2015 International Conference on Energy Systems and Applications*, India, 30 Oct. – 01 Nov, pp. 214-219 (2015). https://doi.org/10.1109/ICESA.2015.7503342

26. Öncü, S. and Sazak, B.S. "Power control of single switch inverter with deleting some control pulses", *J. Fac. Arch. Gazi Univ.*, **21**(1), pp. 123-127 (2006).

27. Karafil, A., Özbay, H., and Öncü, S. "Comparison of regular and irregular 32 pulse density modulation patterns for induction heating", *IET Power Electronics*, **14**(1), pp. 78-89 (2021). https://doi.org/10.1049/pel2.12012

28. Oncu, S., Unal, K., and Tuncer, U. "Laboratory setup for teaching resonant converters and induction heating", *Engineering Science and Technology, an International Journal*, **28**, pp. 1-7 (2022). https://doi.org/10.1016/j.jestch.2021.05.016

29. Chelladurai, B., Sundarabalan, C.K., Santhanam, S.N., et al. "Interval type-2 fuzzy logic-controlled shunt converter coupled novel high-quality charging scheme for electric vehicles", *IEEE Transaction on Industrial Informatics*, **17**(9), pp. 6084-6093 (2021). https://doi.org/10.1109/TII.2020.3024071

30. Nacar, S. and Öncü, S. "Hydrogen production system with fuzzy logic-controlled converter", *Turk. J. Elec. Eng. & Comp. Sci.*, **27**(3), pp. 1885-1895 (2019). https://doi.org/10.3906/elk-1805-77

31. Chang, C.J., Chiang, T.H., and Tai, C.C. "A modified self-tuning fuzzy logic temperature controller for metal induction heating", *Review of Scientific Instruments*, **91**(6), pp. 1-12 (2020). https://doi.org/10.1063/5.0006019

32. Gheibi, A., Mohammadi, S.M.A., and Farsangi, M.M. "A proposed maximum power point tracking by using adaptive fuzzy logic controller for photovoltaic systems", *Scientia Iranica D*, **23**(3), pp. 1272-1281 (2016). https://doi.org/10.24200/sci.2016.3895

33. Komatsu, W.P.W. "A simple and reliable class-E inverter for induction heating applications", *International Journal of Electronics*, **84**(2), pp. 157-165 (1998). https://doi.org/10.1080/002072198134922

34. Borekci, S. and Oncu, S. "Switching-mode BJT driver for self-oscillated push-pull inverters", *Journal of Power Electronics*, **12**(2), pp. 242-248 (2012). https://doi.org/10.6113/JPE.2012.12.2.242

35. Rudnev, V., Loveless, D., and Cook, R.L. *Handbook of Induction Heating, Theoretical Background*, Ed., 2nd Edn., pp. 51-138, CRC Press, London (2017). https://doi.org/10.1201/9781315117485

Biography

Salih Nacar was born in Kahramanmaraş, Turkey in 1984. He received his BS degree in Electronics Teaching in Gazi University, Ankara, Turkey in 2008 and his MS and PhD degrees in Electrical-Electronic Engineering in Karabük University, Karabük, Turkey in 2014 and 2019, respectively. He is currently an Assistant Professor at the Department of Electrical Engineering, Bandırma Onyedi Eylül University. He has published a lot of journal and conference papers in the area of power electronics. His current research interests include power converters, soft switching, control of power converters, renewable energy, high frequency power conversion and induction heating.